AIMS Materials Science, 9(2): 184–213.
DOI: 10.3934/matersci.2022012
Received: 24 November 2021
Revised: 13 January 2022
Accepted: 25 January 2022
Published: 16 February 2022

http://www.aimspress.com/journal/Materials

Review

Polymer based membranes for propylene/propane separation: CMS, MOF and polymer electrolyte membranes

Xiao Yuan Chen[1,2], Anguo Xiao[1] and Denis Rodrigue[1,2,*]

[1] College of Chemistry and Materials Engineering, Hunan University of Arts and Science, Changde, China
[2] Department of Chemical Engineering, Université Laval, Quebec City, Quebec, Canada

* **Correspondence:** Email: Denis.Rodrigue@gch.ulaval.ca.

Abstract: Propylene/propane separations are generally performed by distillation which are energy intensive and costly to build and operate. There is therefore high interest to develop new separation technologies like membrane modules. In our previous paper, we collected, analyzed and reported data for neat polymers and mixed matrix membranes (MMM) based on flat and hollow fiber configurations for propylene/propane separations. In this second part, we collected the data for carbon molecular sieving (CMS) membranes from polymer pyrolysis reaction and metal-organic framework (MOF) membranes from different fabrication methods, as well as data on facilitated transport membrane-polymer electrolyte membranes (PEM). CMS membranes show great potential for C_3H_6/C_3H_8 separation with an optimum pyrolysis temperature around 500–600 °C. However, physical aging is a concern as the micro-pores shrink over time leading to lower permeability. The performance of MOF membranes are above the 2020 upper bound of polymer-based membranes, but have limited commercial application because they are fragile and difficult to produce. Finally, facilitated transport membranes show excellent propylene/propane separation performance, but are less stable compared to commercial polymeric membranes limiting their long-term operation and practical applications. As usual, there is no universal membrane and the selection must be made based on the operating conditions.

Keywords: propylene; propane; separation; membrane; selectivity; permeability; aging effect; carbon molecular sieving; metal-organic framework; facilitated transport

Abbreviations: $AgBF_4$: Silver tetrafluoroborate; $AgNO_3$: Silver nitrate; Al_2O_3: Aluminum oxide; $AI(NO_3)_3$: Aluminum nitrate; 6FDA: 4,4-(hexafluoroisopropylidene)diphthalic anhydride; APAF: 2,2-bis(3-amino-4-hydroxyphenyl)-hexafluoropropane; BPDA: 3,3-4,4-biphenyltetracarboxylic dianhydride; BTESA: Bis(triethoxysilyl)acetylene; BTESB: Bis(triethoxysilyl)benzene; CF_3SO_3: Triflate; DABA: 4,4′-diaminobenzanilide; DAM: 2,4,6-trimethyl-1,3-phenylinediamine; DAT1-OH: 2,6(7)-dihydroxy-3,7(6)-diaminotriptycene; DDBT: Dimethyl-3,7-diaminodiphenylthiophene-5,5-dioxide; LLDPE: Linear low density polyethylene; Matrimid® (BTDA-DAPI): 3,3,4,4-benzophenone tetracarboxylic dianhydride and 5(6)-amino-1-(4-aminophenyl)-1,3-trimethylindane; ODA: 4,4-oxydianiline; PE: Polyethylene; PEBAX: Polyether block amide; PEO: Poly(ethylene oxide); PEP: Poly(ethylene phthalate); PEI: Polyetherimide; PDMS: Polydimethylsiloxane; PMMA: Poly(methyl methacrylate); PI: Polyimide; PIM: Polymers of intrinsic microporosity; POZ: Poly(2-ethyl-2-oxazoline); PU: Polyurethane; PVA: Poly(vinyl alcohol); PVDF-HFP: Poly(vinylidene fluoride-co-hexa fluoropropylene); PVMK: Poly(vinyl methyl ketone); PVP: Poly(vinyl pyrrolidone); PS-b-P4VP: Polystyrene-block-poly(4-vinylpyridine); SbF_6: Hexafluorantimonate; TiO_2: Titanium dioxide; Torlon®: AI-10 poly(amide-imide) precursor as supplied (subsequently imidized); VTMS: Vinyltrimethoxysilane; $Zn(CH_3COO)_2$: Zinc acetate dehydrate; $ZnCl_2$: Zinc chloride anhydrous; $Zn(NO_3)_2$: Zinc nitrate hexahydrate

1. Introduction

In the first part of this study, we compared different polymer-based membranes for propylene/propane separation [1]. Propane and propylene are highly important energy resources and raw materials for industrial chemistry. For example, propane is highly used for industrial and household energy source, while propylene is a starting molecule to synthesize several chemicals and polymers. But propylene/propane (C_3H_6/C_3H_8) separations are mainly carried out by expensive distillation operations which are energy-intensive due to the similar properties of both molecules. Therefore, there is a great interest in the development of new separation technologies that may result in substantial energy savings and large cost reductions. We collected and analyzed the data for neat polymers and mixed matrix membranes (MMM) under different conditions for C_3H_6/C_3H_8 separations. In general, membrane gas separations are based on two mechanisms: physical and chemical. The solution-diffusion mechanism in polymer-based membranes, for which the base theory is associated to a network structure, and molecular sieving mechanism in membranes with different structures are physical mechanisms [2]. An example of a chemical mechanism is facilitated transport in carrier-based membranes which include a chemical reaction [2]. The concept of "solution-diffusion" for gas transport in polymeric membranes was described in our earlier work. On the other hand, molecular sieving effect is related to the aperture being between the sizes of two gas molecules, so only the smaller molecules can diffuse through the pores while the larger ones are rejected. The ideal situation is when a membrane is filled with such pores of uniform size leading to a molecular sieving effect allowing the penetration of only the smaller molecules. However, the presence of structural defects, orientation and other interactions in real cases do not produce ideal molecular sieving conditions. In general, the membrane may exhibit a sudden fall in gas permeance with increasing kinetic diameter of the gas molecules. For example, the gas permeability of ZIF-8 has been reported in two articles [3,4]. The permeability is above 1000 Barrer for smaller gas molecules (H_2, CO_2, Ar, O_2, Kr, N_2, CH_4, C_2H_4 and C_2H_6), but drops from 250 Barrer to 2.8 Barrer

going from C_3H_6 (4.0 Å) to C_3H_8 (4.3 Å), while larger molecules (C_4H_{10}, i-C_4H_{10} and SF_6) have values around 1 Barrer.

The molecular sieving effect is associated with a diffusion dominated penetration process. Molecular sieves can be classified in two broad categories: amorphous (carbon molecular sieves (CMS) and ceramic materials) and crystalline (zeolites and metal-organic frameworks (MOF)) [5]. CMS membranes are generally fabricated via the pyrolysis of polymer precursors under controlled atmosphere and temperature. On the other hand, MOF membranes are microporous crystalline materials with high porosity (up to 90%) [6]. MOF are composed of ordered and infinitely extended coordinated interconnections between metal ions or metal-containing clusters (serving as nodes) and multidentate organic ligands (serving as struts). In particular, ZIF-8 was shown to be very effective for propylene/propane separation because of its suitable crystallographic pore aperture. Both membrane types will be reviewed and compared in terms of their preparation and performance.

2. Background

2.1. Molecular sieving

Based on the solution-diffusion theory, the permeability (P_i) of a gas is the product between its solubility coefficient (S_i) and its diffusion coefficient (D_i) as Eq 1:

$$P_i = S_i D_i \tag{1}$$

A widely used and accepted unit for permeability is the Barrer (1 Barrer = 10^{-10} cm^3 (STP) $cm^{-1}\cdot s^{-1}$ $cmHg^{-1}$) or in international units: mol $Pa^{-1}\cdot s^{-1}\cdot m^{-1}$ (1 Barrer = 3.35 × 10^{-16} $mol\cdot m^{-1}\cdot s^{-1}$). Permeance values are commonly reported in GPU (gas permeation units) defined as 1 GPU = 1 Barrer/1 micron = 10^{-6} cm^3 (STP) $cm^{-2}\cdot s^{-1}\cdot cmHg^{-1}$ (1 GPU = 3.35 × 10^{-10} $mol\cdot m^{-2}\cdot s^{-1}\cdot Pa^{-1}$).

From Eq 1, the ideal selectivity (α) is defined as the product between the diffusion and solution selectivity as Eq 2:

$$\alpha = \frac{P_A}{P_B} = \left(\frac{D_A}{D_B}\right)\left(\frac{S_A}{S_B}\right) \tag{2}$$

The diffusion coefficient (D_i) can be expressed by Eq 3 as an Arrhenius relationship [7]:

$$D_i = D_{i0}\exp\left(-\frac{E_d}{RT}\right) \tag{3}$$

where R is the molar gas constant and T is the absolute temperature, while D_{i0} and E_d are the pre-exponential factor and activation energy for the diffusion of penetrant i, respectively. Furthermore, according to the transition state theory, the pre-exponential factor can be expressed as Eq 4:

$$D_{i0} = e\lambda^2\frac{kT}{h}\exp\left(\frac{S_d}{R}\right) \tag{4}$$

where λ is the average diffusive jump length, S_d is the activation entropy of diffusion, k is Boltzmann's constant and h is Planck's constant. Combining Eqs 1–4, the diffusion selectivity for a pair of gas molecules A and B is given by Eq 5:

$$\frac{D_A}{D_B} = \left(\frac{\lambda_A^2}{\lambda_B^2}\right) \exp\left(\frac{\triangle S^*_{D(A,B)}}{R}\right) \exp\left(\frac{\triangle H^*_{D(A,B)}}{RT}\right) \quad (5)$$

where H* is the enthalpy and S* is the entropy, while $\Delta H^*_{D(A,B)}$ and $\Delta S^*_{D(A,B)}$ are the differences in diffusion transition state enthalpy and entropy for component A versus B, respectively. In other words, the diffusion selectivity is composed of an enthalpic selectivity and entropic selectivity contribution [8]. Eq 5 also indicates that diffusion is controlled by the diffusion activation entropy and the diffusion activation energy. The activation energy refers to the energy required for the molecule to move from the ground state to the activated state: the smaller the size of molecules, the lower the energy required and the lower the activation energy. On the other hand, the activation entropy refers to the change of standard entropy of the gas molecules from their ground state to their diffusion activation state, which is related to the geometric size and the shape of gas molecules. For molecular sieving, the micropore properties, including size, shape and geometry, are very important, as well as the conformation/shape of each gas molecule.

2.2. Facilitated transport

Facilitated transport membranes incorporate a reactive carrier in the membrane leading to a chemical-based reaction mechanism. The carrier reacts with and helps to transport one of the feed components across the membrane. Olefins are able to form reversible chemical bonds with transition metal ions (especially silver, copper and gold) due to the specific interaction between the olefin's hybrid molecular orbitals and the metal's atomic orbitals, commonly known as π-bonding. The bonds formed between transition metal ions and olefins are stronger than those formed by van der Waals forces alone, so it is possible to achieve high selectivity and high capacity for the component to be bound (Eqs 6,7). At the same time, the bonds are still weak enough to be broken by a simple modification of the operating conditions, such as increasing the temperature or decreasing the pressure [9].

$$A_g^+ + \text{olefin} \rightleftarrows A_g^+(\text{olefin})_1 \quad (6)$$

$$\text{olefin} + A_g^+(\text{olefin})_1 \rightleftarrows A_g^+(\text{olefin})_2 + \text{olefin} \quad (7)$$

Among the transition metals, the complexation of silver (Ag) is prominent as its electronegativity is 2.2, which is in a suitable range of electronegativity (1.6–2.3) for reversible complexation by the optimization of experimental conditions [10]. The reason for this optimum range is a balance between the forward and reverse reactions. The higher the electronegativity of the metal, the stronger the π bond formed with the olefin and the more difficult it is to reverse this interaction. But when the metal electronegativity is too low, interactions with the olefin are weak and not suitable as a carrier [11]. Moreover, silver salts have the lowest lattice energy compared with other metal salts used for facilitated transport. This low lattice energy is beneficial to improve the solubility of metal cations, therefore improving interactions with olefins [12].

The transport of propylene through a membrane is the result of two different mechanisms simultaneously acting as illustrated in Figure 1. When propylene and propane are in contact with a non-porous material, the gas molecules must first solubilize in the polymer matrix. The absorbed

molecules then diffuse through the membrane according to the solution-diffusion theory. But when silver ions are present in the membrane, complexation takes place between the olefin molecules and the Ag^+ cations that are partially coordinated with the polymer matrix. In this case, the olefin simply follows a hopping mechanism to reach the other side of the membrane [10].

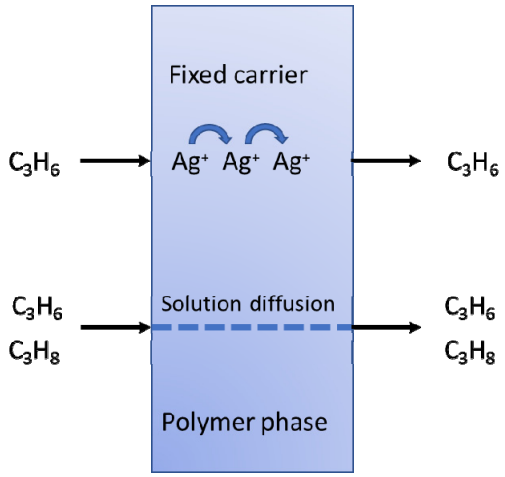

Figure 1. Schematic representation of the mechanisms inside a separation membrane including facilitated transport [10].

3. Membranes

3.1. CMS membranes

In order to improve the performance and reduce the plasticization effect in polymer membranes for C_3H_6/C_3H_8 separations, carbon molecular sieve (CMS) membranes were developed. CMS membranes have shown exceptional gas separation performance due to their highly rigid and slit-like pore structure suitable for size exclusion of gases with similar physical properties like ethylene/ethane (C_2H_4/C_2H_6) or propylene/propane (C_3H_6/C_3H_8) [13,14]. In addition, CMS membranes have shown good plasticization resistance and high C_3H_6/C_3H_8 mixed-gas selectivity [13,14].

CMS membranes are generally prepared by the carbonisation or pyrolysis of appropriate precursor polymer membranes. The polymers may be cellulose acetate (CA), poly(vinylidene chloride) (PVDF), polyimides (PI), poly(furfuryl alcohol) (PFA) and phenolic resins (PR) [15]. The precursor polymers are pyrolyzed in an ultra-high purity argon (Ar) gas atmosphere using an oxygen (O_2) removal assisted pyrolysis setup to form CMS membranes. Oxygen levels in the pyrolysis quartz tube are monitored by an oxygen sensor due to the high impact of oxygen traces on the CMS membrane transport properties [16]. Typical pyrolysis temperature is around 550–600 °C, but temperatures up to 800–1000 °C have been reported.

Suda et al. [17] prepared CMS membranes by vacuum pyrolysis from Kapton polyimide films at 1000 °C and then activated the membranes in water vapor to slightly enlarge the pores. The resulting CMS membrane showed a pure gas C_3H_6/C_3H_8 selectivity of 20. Steel and Koros investigated the effects of polymer precursors (6FDA/BPDA-DAM, 4,4-

(hexafluoroisopropylidene)diphthalic anhydride (6FDA), 3,3-4,4-biphenyltetracarboxylic dianhydride (BPDA), 2,4,6-trimethyl-1,3-phenylinediamine (DAM) and Matrimid® 5218 (3,3,4,4-benzophenone tetracarboxylic dianhydride and 5(6)-amino-1-(4-aminophenyl)-1,3-trimethylindane)) and pyrolysis conditions on the gas separation properties of dense flat CMS membranes [18,19]. Table 1 shows that for larger molecules, such as the C_3H_6/C_3H_8 pair, the effect of the final pyrolysis temperature is clearly different from smaller gas pairs like CO_2/CH_4. As the temperature increased from 550 to 800 °C, the CO_2 permeability decreased from 1000 to 90 Barrer, the CO_2/CH_4 selectivity increased from 40–70 to 200, while the C_3H_6 permeability for 800 °C CMS was 0.1 Barrer and the C_3H_6/C_3H_8 selectivity was 4.4. The reason for this difference may be that the ultramicropore volume is reduced due to densification. The average ultramicropore sizes are sufficiently small to exclude the passage of both propylene and propane through most of these pores. Similar results were observed for 6FDA/BPDA-DAM. In the case of C_3H_6/C_3H_8 separation, a pyrolysis temperature of 500 °C yielded much better performances than 800 °C.

Table 1. Permeation properties of polymer precursor and CMS membranes at 35 °C and feed pressures less than 100 psia [18,19].

Materials	Pyrolysis conditions	P_{C3H6} (Barrer)	P_{C3H6}/P_{C3H8} (-)
Matrimid	-	0.1	10
Matrimid	550 °C, 2 h	9.1	5.8
Matrimid	800 °C, 2 h	0.1	4.4
Matrimid	500 °C	13	40
6FDA/BPDA-DAM	-	11.8	13
6FDA/BPDA-DAM	500 °C 2 h	196	100
6FDA/BPDA-DAM	800 °C, 2 h	1.3	7.9

Xu et al. [13] prepared CMS membranes derived from Matrimid® and 6FDA/BPDA-DAM hollow fibers pyrolyzed at 550 ^{o}C. The results showed that the "slit-like" structures of CMS enabled the separation of bulk olefins (C_3H_6) from paraffins (C_3H_8). The CMS dense flat membrane based on Matrimid and 6FDA/BPDA-DAM showed a C_3H_6 permeability of 0.1 and 11.8 Barrer and a C_3H_6/C_3H_8 selectivity of 10 and 13 at 35 °C and 100 psig. CMS based on Matrimid and 6FDA/BPDA-DAM hollow fiber membranes showed a permeance of 0.76 and 17.5 GPU with a selectivity of 21 and 20.5 at 35 °C and 50 psig. The authors reported that CMS hollow fibers derived from Matrimid suffered a substructure collapse during the intense heat treatments leading to an increase of the effective separation layer thickness and reduced permeance. Since 6FDA/BPDA-DAM hollow fiber membranes have higher glass-rubber transition temperatures compared to Matrimid, they could overcome this substructure collapse problem.

Then, Xu et al. used the same materials to determine why the substructure collapse occurred [20]. Polymer chain flexibility (relatively low glass transition temperature (Tg) for Matrimid® compared to 6FDA/BPDA-DAM CMS) appears to be the main origin of the substructure collapse. This phenomenon must be addressed in all cases involving high heat treatment near or above Tg. Since heat is transferred from the skin side to the bore side, collapse firstly occurs at the outer layer. The authors proposed to overcome this permeance loss problem by selecting a high Tg precursor, but the pyrolysis process and the hollow fiber formation step also need further study.

The V-treatment technique was also proposed to overcome the substructure collapse [21]. The precursor fibers, after the solvent exchange step, were firstly saturated with vinyltrimethoxysilane (VTMS) before being exposed to moisture at 25 °C. A silane-moisture reaction created some organic

crosslinked silica on the fibers pore walls via a sol-gel crosslinking reaction. This technique enabled to limit, at least at the microscale, a morphology collapse for asymmetric CMS membranes without a chemical reaction. The result showed that the skin thickness significantly decreased for Matrimid (from 40 to 5–6 μm) and 6FDA:BPDA-DAM (from 16–17 to 3–4 μm) compared to CMS without a V-treated precursor. This significant change in membrane skin thickness directly increases the gas permeance for both asymmetric CMS V-treated hollow fibers. However, no permeation data were reported to separate propylene from propane.

Thermally-rearranged (TR-440 ^{o}C) and carbon molecular sieve (CMS-600 ℃) membranes made from an intrinsically microporous polymer precursor PIM-6FDA-OH (polymers of intrinsic microporosity, PIM) were reported for the separation of propylene from propane (Figure 2) [14]. Thermally-rearranged (TR-440 ℃) PIM-6FDA-OH membrane showed good permeability compared to the precursor PIM-6FDA-OH for C_3H_6/C_3H_8 separation. The CMS membrane had excellent pure gas performance with a C_3H_6/C_3H_8 selectivity of 33 coupled with a C_3H_6 permeability of 45 Barrer. For mixed-gas conditions, a C_3H_6/C_3H_8 selectivity of 17 and C_3H_6 permeability of 31 Barrer at 4 bar feed pressure was reported. No evidence of plasticization was observed under these conditions (Table 2).

Another intrinsically microporous hydroxyl-functionalized polyimide (6FDA-DAT1-OH) made from 6FDA and DAT1-OH (2,6(7)-dihydroxy-3,7(6)-diaminotriptycene) was thermally converted at 460 ℃ for 30 min leading to a 100-fold increase in C_3H_6 permeability to 39 Barrer and a C_3H_6/C_3H_8 selectivity of 23. The conversion of the 6FDA-DAT1-OH polyimide precursor to TR-6FDA-DAT1-OH derivatives was confirmed via TGA-MS and FTIR. TR polymers contained the same backbone structure compared to the precursor, but hydroxyl groups were left (Figure 2). The TR polymer has increased free volume which was reflected by increased microporosity as determined by enhanced Brunauer-Emmett-Teller (BET) surface area from 167 to 405 $m^2 \cdot g^{-1}$. After 28 d of physical aging, the 6FDA-DAH1-OH-460-30 membrane performance decreased as the C_3H_6 permeability dropped to 21 Barrer with a simultaneous decrease in C_3H_6/C_3H_8 selectivity to 16. The performance was also reduced for mixed-gas with a C_3H_6 permeability of 12.8 Barrer and a C_3H_6/C_3H_8 selectivity of 8. Physical aging is a naturally occurring phenomenon in glassy polymers leading to a densification of the polymer matrix trying to reach an equilibrium state. This phenomenon leads to a loss of gas permeability over time [22]. Smith et al. [23] performed a similar thermal rearrangement of 6FDA-APAF (2,2-bis(3-amino-4-hydroxyphenyl)-hexafluoropropane) polyimide (450 ℃) and reported a pure C_3H_6 permeability of 17 Barrer with a C_3H_6/C_3H_8 selectivity of 16.

Karunaweera et al. [24] used a high molecular weight crosslinkable polyimide (6FDA-DABA 4,4′-diaminobenzanilide) to produce CMS membranes. The pyrolysis temperature was 350 ℃ for 2 h or 450 ℃ for 2 h, then 550 ℃ for 2 h. The best results for pure gas permeabilities were in excess of 403 Barrer with propylene/propane selectivities as high as 25 for 6FDA-DABA-450-550 (Table 2). Mixed-gas (C_3H_8:C_3H_6 50:50) measurements yielded a propylene permeability of 257 Barrer and a selectivity of 20 for the same membrane.

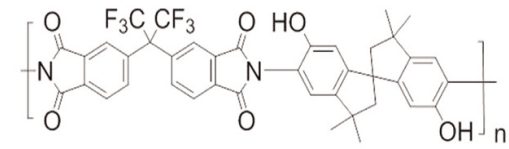

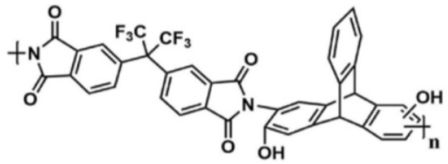

Figure 2. Chemical structure of PIM-6GDA-OH and 6FDA-DAT1-OH.

Table 2. Pure gas and mixed-gas C_3H_6/C_3H_8 transport properties of PIM-6FDA-OH, TR, CMS and 6FDA-DAT1-OH, TR, CMS membranes.

Membrane	P_{C3H6} (Barrer) (pure gas)	$P_{C3H6/PC3H8}$ (pure gas)	P_{C3H6} (50:50 C_3H_6:C_3H_8) (Barrer)	$\alpha_{C3H6/C3H8}$ (50:50 C_3H_6:C_3H_8)	Test conditions (℃/bar)	Ref.
PIM-6FDA-OH-250 ℃	3.5	30	-	-	35/2	[14]
PIM-6FDA-OH-440 ℃	14	15	11	11	35/2	[14]
CMS-600 ℃	45	33	31	17	35/2	[14]
6FDA-DAT1-OHa	0.3	33	-	-	35/4	[22]
6FDA-DAT1-OH-460-30min	39	23	-	-	35/2	[22]
6FDA-DAT1-OH-28d	21	16	12.8	8	35/2	[22]
6FDA-APAF-450	17	16	-	-	35/2	[23]
6FDA-DABA	0.05	0.013	-	-	35/3.3	[24]
6FDA-DABA-550	378	12.8	-	-	35/3.3	[24]
6FDA-DABA-350-550	390	21.2	-	-	35/3.3	[24]
6FDA-DABA-450-550	403	25.4	257	20	35/3.3	[24]

Okamoto et al. [25] prepared CMS membranes by pyrolyzing an asymmetric hollow fiber polymer membrane of BPDA-DDBT/DABA (dimethyl-3,7-diaminodiphenylthiophene-5,5-dioxide DDBT). The membranes pyrolyzed at 600–630 ℃ exhibited a high permeance of 26 GPU for C_3H_6 at 35 ℃ and 1 atm. However, a relatively low selectivity (11) for a C_3H_6/C_3H_8 mixture separation was observed.

Askari et al. [26] made thermally crosslinkable PI (400 ℃) two-layer hollow fiber membranes grafted with β-cyclodextrin. The results showed that without a silicon rubber coating, the sample 6FDA-Durene-400 displayed the best C_3H_6/C_3H_8 separation with a C_3H_6 permeance of 73 GPU and a selectivity of 10.5. After silicon rubber coating addition, the best selectivity was 15.3 with a C_3H_6 permeance of 29 GPU.

Hayashi et al. [27] prepared CMS membranes by pyrolysis of BPDA/ODA polyimide coated on porous alumina tubes (substrate) at 600–900 ℃ in a nitrogen stream. They reported good

performances with a propylene permeance of 2.4 and 9 GPU combined with a selectivity of propylene over propane of 46, 33 and 35 at 100 ℃ for the membranes pyrolyzed at 700 ℃ and 101.3 kPa.

Ma et al. [28,29] reported CMS (6FDA-based polyimide) also formed on the surface of alumina supports by dip-coating in a polymer solution. The supported polymer films were dried at room temperature for 3 h, then at 100 ℃ for 12 h and finally annealed at 140 ℃ for 5 h before conducting pyrolysis. The membranes were then pyrolyzed at a temperature between 550 and 750 ℃. The thermal ramps (heat and cool) were set at 4 ℃/min. For tests performed at 25 ℃ and a total feed pressure of 23.5 psi (162 kPa), the membrane showed a gas mixture (50/50 C_3H_6/C_3H_8) selectivity of 35 and a C_3H_6 permeance of 8.1 GPU on mesoporous γ-alumina supports. The authors considered that the permeation/separation properties of CMS membranes strongly depended on the test temperature and exposure time as the propylene permeance increased (about 3 fold) by increasing the temperature (25 to 100 ℃). The permeance of propylene and propane also decreased, while the propylene/propane selectivity slightly increased for the first 10 d. Thereafter, the separation properties stabilized when exposed to a gas mixture. The authors reported that the micropores in CMS membranes, derived from large free volume polymers, tended to shrink over time to reach a thermodynamically more stable state, resulting in lower permeance and higher selectivity. This physical aging of CMS membranes causing structural pore changes was firstly reported by Koros and coworkers [30].

Kim et al. [31] investigated thin carbon molecular sieve membranes deposited on alumina hollow fibers. Firstly, the porous α-alumina hollow fibers were prepared via an extrusion spinning process. Then, an intermediate alumina layer was introduced onto the hollow fiber. Finally, a thin layer of Matrimid® 5218 was coated on the support fiber for a final pyrolysis temperature of 650 ℃. The resulting CMS membrane exhibited a C_3H_6 permeance of 45 GPU and a C_3H_6/C_3H_8 selectivity of 16.5 for mixed gas and the separation performance for this single-component permeance was 80 GPU for C_3H_6 and 30 for the ideal gas selectivity of C_3H_6/C_3H_8 (Table 3) [28]. The authors considered that this type of CMS had some advantages in separation performance and physical strength compared to unsupported membranes. Similar CMS structures have also been developed. For example, Ma et al. prepared CMS membranes on alumina disks and measured their separation properties for propylene/propane mixtures [32]. Teixeira et al. reported the preparation of CMS membranes on alumina tubes from boehmite-loaded phenolic resin [33]. These results were obtained by a cross-flow setup which is a mixture between a gas flow on the feed side and N_2 as a sweep gas on the permeate side which were different for each measurement.

Table 3. Pure gas and mixed-gas permeation properties of CMS hollow fiber membranes.

Membrane	P_{C3H6} (GPU) (pure gas)	P_{C3H6}/P_{C3H8} (pure gas)	P_{C3H6} (GPU) (50:50 C_3H_6:C_3H_8)	$\alpha_{C3H6/C3H8}$ (50:50)	Ref.
Matrimid-550	0.76	21	-	-	[13]
6FDA/BDPA-DAM-550	17.5	20.5	-	-	[13]
BPDA-DDBT/DABA-600	26	11	-	-	[25]
6FDA-Durene-400	73	10.5	-	-	[26]
6FDA-Durene-400-PDMS	29	15.3	-	-	[26]
BPDA/ODA-700	2.4, 9.0	46, 35	-	-	[27]
6FDA-based-550	-	-	8.1	35	[28,29]
Matrimid-650	80	30	45	16.5	[31]

The group of Koros studied the effect of post-aging thermal-treatment for CMS hollow fiber membranes based on 6FDA:BPDA/DAM [34,35]. The precursor polymer hollow fibers were prepared by a dry-jet/wet-quench spinning process before the fibers were pyrolyzed from 50 to 250 ℃ at 10 ℃/min, then to 660 ℃ at 3 ℃/min before increasing to 675 ℃ at 0.25 ℃/min under an ultra-high purity (UHP) argon stream. After soaking at 675 ℃ for 2 h, the furnace was shut down and natural cooling to 50 ℃ occurred under a continuous argon purge. Finally, a post-pyrolysis thermal treatment of the CMS fibers was performed at higher temperature (250–300 ℃); i.e. super-hyperaging. The pristine CMS fiber without post-pyrolysis showed C_3H_6 permeances of 19.8 GPU with C_3H_6/C_3H_8 separation factors of 22.6. When the CMS modules were stored under ambient air conditions for 3 months, the C_3H_6 permeance dropped to 0.3 GPU while the C_3H_6/C_3H_8 separation factors increased to 35 due to an aging effect. When CMS hollow fibers were firstly hyperaged at 110 ℃ for 18 h in air, a C_3H_6 permeance of 0.19 GPU with a C_3H_6/C_3H_8 separation factor of 60.6 were observed (Table 4). The hyperaged fibers were then super-hyperaged at a temperature between 250 and 300 ℃ for different time under air as shown in Table 5. Unfortunately, the authors observed that the super-hyperaging regenerated CMS fibers were still ageing. Therefore, they proposed a "re-aging" of the super-hyperaging regenerated CMS fibers by imposing again 280 ℃ for 30 min. A C_3H_6 permeance of 30.5 GPU with a C_3H_6/C_3H_8 selectivity of 12.8 was reported showing the possibility to highly recover the initial separation performance (C_3H_6 permeance = 19.8 GPU, $\alpha_{C3H6/C3H8}$ = 22.6).

Table 4. Separation properties of CMS fibers as a function of super-hyperaging conditions [35].

Super-hyperaging temperature (℃)	Super-hyperaging time (min)	C_3H_6 permeance (GPU)	$\alpha_{C3H6/C3H8}$
Pristine CMS fiber	-	19.8	22.6
Hyperaging 110	18	0.19	60.6
300	60	70.5	7.2
300	30	31.6	7.0
300	20	8.1	13.3
280	45	12.5	20.6
280	30	25.8	9.7
280	20	24.9	10.7
250	30	6.2	45.4
Re-280	30	30.5	12.8

The precursors bis(triethoxysilyl)acetylene (BTESA) and bis(triethoxysilyl)benzene (BTESB) were selected in the production of organosilica (plane composite) membranes for propylene/propane separation. Guo et al. [36,37] firstly prepared the organosilica sols via hydrolysis and polymerization reactions using BTESA and BTESB as precursors. Then, a porous α-alumina tube was produced followed by calcination at 550 ℃ for 20 min as a support. Finally, the (composite) organosilica sols were diluted to 0.25 wt% with EtOH. They were coated and calcinated directly on the surface of the tube at 300 ℃ under a N_2 atmosphere for 30 min. The results of single and mixed gas transport properties are reported in Table 5. It is interesting to see that the C_3H_6/C_3H_8 separation from a single to a binary-gas permeation system was improved. This was attributed to the blockage of C_3H_8 permeation since the C_3H_6 was preferentially absorbed. The authors considered that a suitable or moderate pore sizes (0.45–0.52 nm) can blocked C_3H_8 even if the C_3H_6 permeability was slightly

decreased so the selectivity increased for the binary systems [36,37]. These data are compared with other CMS hollow fiber membranes for pure gas in Figure 3

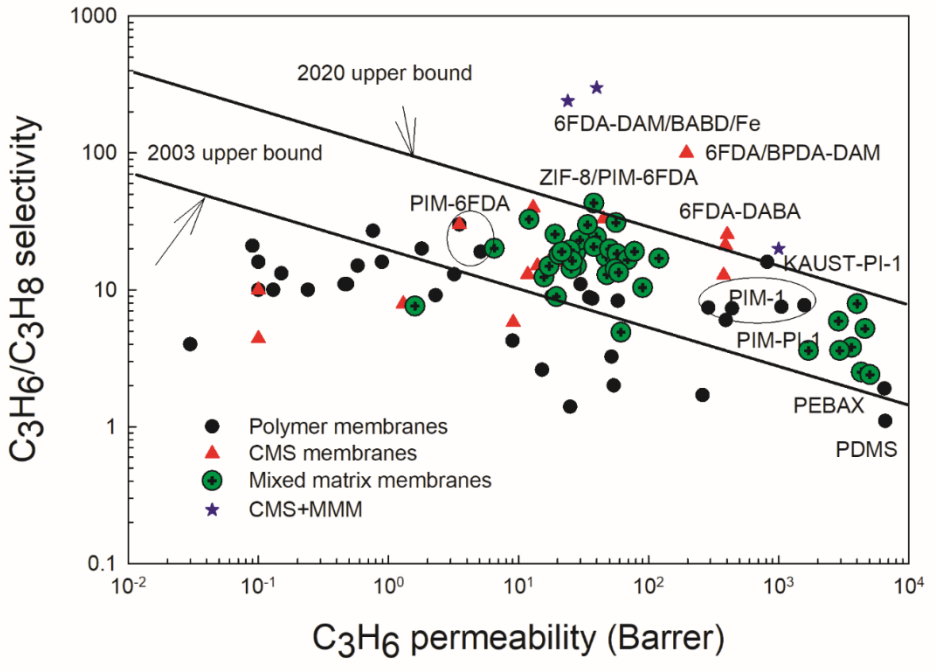

Figure 3. Pure gas C_3H_6/C_3H_8 separation performance of flat membranes based on neat polymers, carbon molecular sieves (CMS), mixed matrix membranes (MMM) and their combination (CMS+MMM).

Chu and Koros developed CMS dense membranes derived from 6FDA-DAM:DABA (3:2) polyimide precursor with integrated Fe^{2+} (Iron(II) acetylacetonates [$Fe(acac)_2$]) for the separation of C_3H_6 and C_3H_8 [38]. Pyrolyzed at 550 ℃, the CMS membranes with integrated Fe^{2+} (0, 1 and 2 wt% in the precursor) showed excellent selectivity increasing from 20 to 300 and 230. However, the C_3H_6 permeability rapidly decreased from 1000 to 40 and 24 Barrer, respectively. The stability of the Fe-containing CMS was investigated by continuous testing using a 50 psia multicomponent mixed gas at 35 ℃ over a period of 60 d. The results showed a C_3H_6 permeability of 20–30 Barrer and a selectivity between 80 and 400 due to the high C_3H_8 permeability variation. This type of membrane, combining the CMS and MMM advantages, showed excellent performance for propylene and propane separation.

Shin et al. [39] developed PI/LPSQ (80/20 wt./wt.) asymmetric hollow fiber membranes for gas separation, where PI was 6FDA-DAM:DABA (3:2) and LPSQ is a ladder structured-poly(phenyl-co-pyridylethyl)silsesquioxane with a phenyl:pyridylethyl ratio of 6:4 (LPPyr64). The PI and PI-LPSQ membranes were pyrolyzed at 675 ℃ following a standard pyrolysis protocol. The results obtained are presented in Table 5.

Table 5. Pure gas and mixed-gas C_3H_6/C_3H_8 transport properties for BETSA and BETSB plane composite membranes, CMS dense flat of PI and PI-LPSQ membranes.

Membrane	P_{C3H6} pure gas (GPU)	C_3H_6/C_3H_8 selectivity (-)	P_{C3H6} mixed-gas (GPU)	50:50 C_3H_6:C_3H_8 selectivity (-)	Test conditions (°C/bar)	Ref.
BTESA	228	14	200	25	50/2	[36,37]
BETSA/BTESB (9:1)-300	143	22	128	33	50/2	[36,37]
BETSA/BTESB (7:3)-300	14.2	9	-	18	50/2	[36,37]
BTESB-300	8.2	2.5	-	4	50/2	[36,37]
CMS-PI*	630 ± 100	15 ± 3	460 ± 20	10 ± 1	35/1-2	[39]
CMS PI-LPSQ10*	290 ± 60	44 ± 5	270 ± 80	22 ± 8	35/1-2	[39]
CMS PI-LPSQ20*	77 ± 5	67 ± 13	67 ± 20	52 ± 20	35/1-2	[39]

*The unit of single and mixed gas permeation were Barrer for CMS dense flat membranes of PI and PI-LPSQ.

For CMS dense membranes, PI (without LPSQ), PL-LPSQ10 (10 wt% of LPSQ) and PL-LPSQ20 (with 20 wt% of LPSQ), the pure gas selectivities increased from 15 to 67, while the permeabilities decreased. The authors considered that the impermeable SiO_2 phases created by the thermo-oxidative crosslinking and the subsequent etching of siloxanes forming additional effective ultramicropores, resulted in a densification of the nonporous inorganic SiO_2 phases, thus decreasing the C_3H_6 and C_3H_8 permeability. But this also contributed to a significant increase of the C_3H_6/C_3H_8 selectivity. The mixed gas C_3H_6/C_3H_8 separation performances were lower than those of single gas, but considered as good. For the hybrid precursor hollow fiber membranes (HFM), a C_3H_6 permeance of 3.3 GPU and a selectivity of 13 at 1 bar, 35 °C was observed for single gas. The corresponding CMS PI-LPSQ20 HFM aged for 30 d after pyrolysis had a C_3H_6 permeance of 2.9 GPU and a selectivity of 57. For mixed gas, CMS PI-LPSQ20 HFM aged a week after pyrolysis exhibited a C_3H_6/C_3H_8 separation factor of 35 and a moderate C_3H_6 permeance of 4.1 GPU due to physical aging. However, no data on CMS PI-LPSQ20 HFM was reported to compare and the anti-aging effect of impermeable SiO_2 was not clear.

The pure gas C_3H_6/C_3H_8 separation performance of CMS compared to the neat polymer-based flat membranes are summarized in Figure 4. CMS membranes with slit-like structures for the separation of bulk olefins (C_3H_6) from paraffins (C_3H_8) have highly improved performance and several membranes are beyond the 2020 experimentally observed C_3H_6/C_3H_8 upper bound [1]. 6FDA/BPDA-DAM-500 has a C_3H_6/C_3H_8 selectivity of 100 and a C_3H_6 permeability of 196 Barrer. Furthermore, 6FDA-DABA-550, Matrimid-500 and PIM-6FDA-600 are on the 2020 upper bound. Overall, CMS membranes have great potential for C_3H_6/C_3H_8 separation with an appropriate pyrolysis temperature being in the range of 500–600 °C. In particular, 6FDA-DAM:DABA/Fe-550 °C has permeabilities of 40 and 24 Barrer with selectivities of 300 and 230 which are above the upper bound. This membrane, based on 6FDA-DAM:DABA (3:2) polyimide precursor with integrated Fe^{2+} and pyrolyzed at 550 °C, has a good overall performance by combining the advantages of both CMS and MMM.

Similarly, an analysis of the gas permeation data for hollow fiber membranes is presented in Figure 4 [1]. Results including post-aging thermal-treatment of CMS hollow fiber membranes based

on 6FDA:BPDA/DAM were added from the original plot. 6FDA:BPDA/DAM-300 hollow fiber CMS membrane shows one of the best separation performance, while BTESA/BTESB membranes coated and calcinated directly on the surface of an α-alumina tube at 300 ℃ also give interesting results.

Obviously, all the CMS membranes need to be heated to 500–600 ℃ or above in an environment without air. This means that a high amount of energy is consumed and special equipment are necessary. Therefore, these membranes lead to higher fabrication costs compared to neat polymer membranes. Physical aging is a disadvantage for CMS membranes as the micro-pores shrink over time leading to a permeability loss. But for the moment, limited information can be found in the literature. The porous structure collapse is another problem for CMS membranes. This is why a high glass transition temperature (Tg) materials must be selected to further develop the pyrolysis protocol and produced better hollow fibers. This can also be done using other additives/methods.

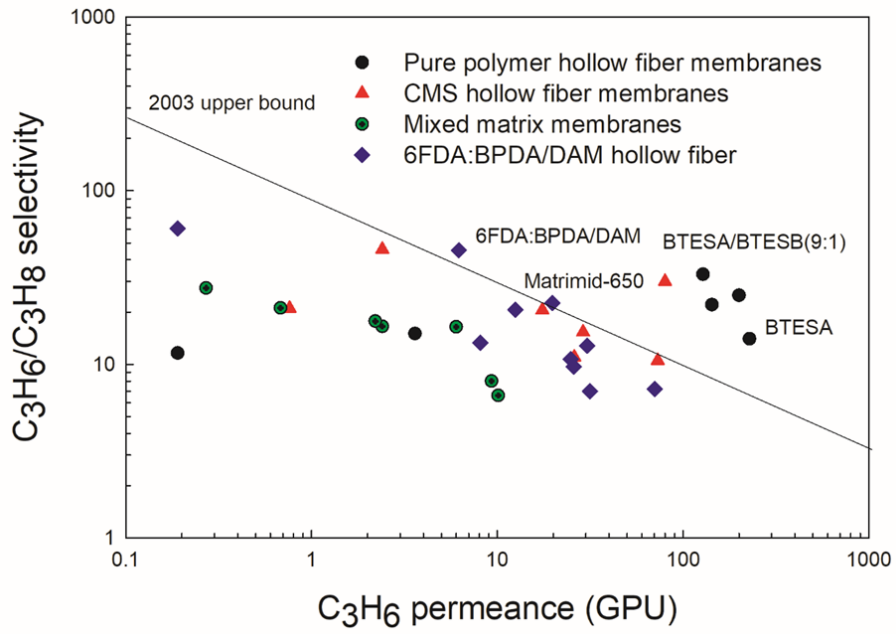

Figure 4. Pure gas C_3H_6/C_3H_8 separation performance of hollow fiber membranes based on neat polymers, carbon molecular sieves (CMS) and mixed matrix membranes (MMM).

3.2. MOF membranes

Zeolites have a similar porous structure as MOF, but they do not belong to MOF or polymer. Zeolite-based membranes are generally made on a ceramic support via in situ or secondary growth methods. In this case, the crystal structure is controlling the micropores. To date, different zeolites have been studied for olefin/paraffin separations. The most important parameter is the pore size which can vary from 7.4 Å for Na-X [36], to 5.5 Å for ZSM-5 and 7.2 Å for ETS-10 [2].

Mundstock et al. [40] reported a Na-X membrane grown on an alumina support modified with 3-aminopropyltriethoxysilane. Their membrane showed only a separation factor of 3.3 for the propylene/propane mixture on the basis of the adsorption selectivity. Therefore, these zeolites should

reduce or eliminate intercrystalline gaps to be suitable for olefin/paraffin (4.3–4.5 Å) separations. Although some methods are effective to decrease the size of these intercrystalline gaps, the permeance of the resulting zeolite membranes is frequently compromised.

Metal-organic frameworks (MOF) are compounds based on metal ions/clusters coordinated with organic ligands to give 1-, 2- or 3-D structures. MOF are similar to zeolites as they are a class of microporous crystalline substances with high porosity (up to 90%) [6]. MOF can also be classified as inorganic-organic hybrid materials.

Among the several types of ZIF, KAUST-1 (Zr-fum-fcu-MOF), ZIF-67, ZIF-90 and ZIF-8 are the most promising candidates for propylene/propane separation, especially the latter because its most effective aperture size for molecular sieving is between 0.40 and 0.42 nm, which corresponds to the kinetic diameters of propylene and propane, respectively [7]. For example, ZIF-8 is composed of zinc atoms connected by imidazolate linkers, 2-methyl imidazole moieties as ligands forming a sodalite structure with large cavities (1.16 nm in diameter), which are connected by small apertures (0.34 nm in diameter) [7,41]. Imidazolate ($C_3H_3N_2^-$) is the conjugate base of imidazole. It is a nucleophile and a strong base (Figure 5).

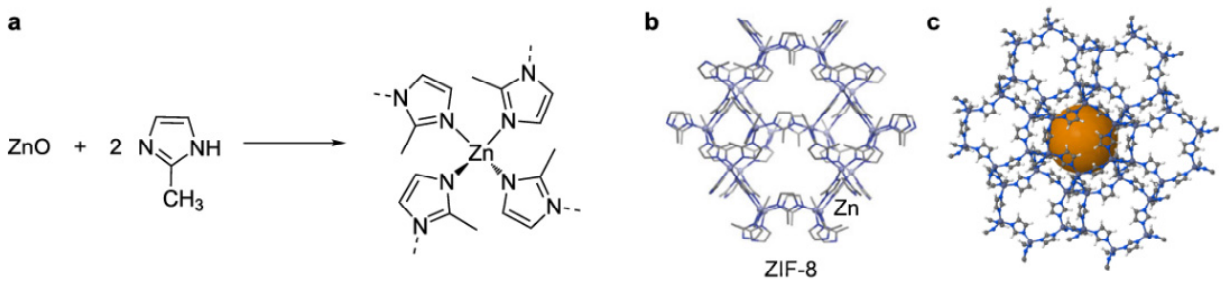

Figure 5. (a) Synthesis of ZIF-8 [41], (b) fragment of the crystal structure of ZIF-8 [42] and (c) image generated for ZIF-8 [43].

Pan et al. were the first in 2012 to report an efficient propylene/propane separation using a ZIF-8 membrane [44]. By applying secondary growth, the membrane showed a propylene permeance of 61.8 GPU and a propylene/propane selectivity of 45. Since then, various methods have been used to fabricate ZIF-8 membranes to improve the separation performance. In 2015, Pan et al. optimized the activation process of ZIF-8 membrane by the same method on homemade α-alumina discs and achieved a separation factor close to 90 for a 50:50 mixture [45]. Liu et al. [46] developed thinner (2.5 μm) ZIF-8 membranes on an α-Al_2O_3 support via secondary growth synthesis in water solution. With equimolar binary feed, the ZIF-8 membranes exhibited consistent C_3H_6/C_3H_8 selectivity of about 30 and C_3H_6 permeance of 1.1×10^{-8} mol/m^2·s·Pa (33 GPU). The permeations were studied by the Wicke-Kallenbach technique with a total feed flow rate of 50 ml/min at atmospheric pressure for single gas or gas mixture (50:50 molar ratio). For C_3H_6/C_3H_8 mixtures, both the permeance and selectivity decreased with increasing feed pressure as the selectivity slightly decreased from 30.1 to 27.0 when the pressure increased from 1 to 5 bar. More information is reported in Table 6 with a comparison with similar works.

Table 6. Mixed-gas C_3H_6/C_3H_8 transport properties for ZIF-8 membranes.

Membrane	Fabrication method*	P_{C3H6} (GPU)	$\alpha_{C3H6/C3H8}$	Thickness (μm)	Test method**	Ref.
ZIF-8	C-D	6.9	57	80	T-LW-K	[7]
ZIF-8	S-G	61.8	45	2.2	W-K	[44]
ZIF-8	S-G	23.4	89	-	W-K	[45]
ZIF-8	S-G	33	30	2.5	W-K	[46]
ZIF-8	IMMP	27	12	8.8 ± 1.4	W-K	[47]
ZIF-8	IMMP	50	160	8.1 ± 1.6	W-K	[47]
ZIF-8	IMMP	66	65	4.5	W-K	[48]
ZIF-8	E-C	54	300	0.2	W-K	[49]
ZIF-8	E-C	182	142	0.5	W-K	[50]
ZIF-8	GVD	840	70	87	W-K	[51]
ZIF-8	GVD	90	150	0.017	T-L	[52]
ZIF-8@ZIF-67@ZIF-8	S-G	111	200	-	W-K	[53]
ZIF-8	S-G	71	105	0.1–0.2	W-K	[54]

*S-G = secondary growth; C-D = counter-diffusion; IMPP = interfacial microfluidic membrane processing; E-C = electrochemical deposition; GVD = gel vapor deposition.

**T-L = time-lag method; W-K = Wicke-Kallenbach technique.

Kwon et al. [55] reported a one-step in situ synthesis (counter-diffusion method) on homemade α-Al_2O_3 disks (porosity = 46%, diameter = 22 mm and thickness = 2 mm) to prepare ZIF-8 membranes. The ZIF-8 membranes were grown at the interface between two disks. The result showed a separation performance for a propylene/propane (50/50) mixture (selectivity ~55) and 100 Barrer of propylene permeability and 50 of selectivity at room temperature and atmospheric pressures for pure gas. Gas permeation tests were performed following the Wicke-Kallenbach (W-K) technique. Propylene/propane single and binary gas permeation measurements were carried out at various temperatures under atmospheric pressure. This was the first time that an inorganic support was used which was extended to polymer-supported ZIF-8 membranes.

In 2014, 80 μm thick ZIF-8 membranes were prepared using a counter-diffusion method on the outermost section of a porous α-alumina capillary substrate [7]. The average permeance of propylene was 2.3×10^{-9} $mol \cdot m^{-2} \cdot s^{-1} \cdot Pa^{-1}$ (6.9 GPU) with an average ideal separation factor for propylene/propane of 57 at 298 K. The gas permeation analyses were conducted from 298 to 363 K using a time-lag method under a high vacuum with a pressure difference of 0.1 MPa.

The group of Nair reported a new route for processing MOF membranes into polymeric hollow fibers by combining a two-solvent interfacial approach for position control over the membrane formation (inner and outer fiber surfaces) resulting in the ZIF-8 membrane being on the inner surface of the hollow fiber with an average membrane thickness of 8.8 μm. This process was called interfacial microfluidic membrane processing (IMMP). Torlon (polyamide-imide, PAI) hollow fibers with a pore size of ~100 nm and room-temperature N_2 permeance of 53000 GPU was used as the support material. A single fiber showed a permeance of 27 GPU and a selectivity of 12 for binary C_3H_6/C_3H_8 separation [56]. This was the first report on IMMP for the preparation of ZIF-8 hollow fiber membranes. In this case, low-cost polymer hollow fibers were used as the supports and continuous molecular sieving ZIF-8 membranes in single or modules hollow fibers was produced. So

IMMP is a promising approach for the scale-up production of MOF-based hollow fiber composite membranes.

In 2016, Eum et al. developed selective ZIF-8 membranes using the same IMMP method on PAI (Torlon) hollow fibers for propylene/propane separation [47,48]. The performance of these engineered ZIF-8 membranes was characterized showing a separation factor of 65 for C_3H_6/C_3H_8 mixtures with C_3H_6 permeances as high as 66 GPU [48]. The authors further optimized the IMMP conditions to better control the fiber microstructure leading to a separation factor of up to 180 (1 bar, $\Delta P = 0$ bar and 25 °C), which remained as high as 60 at 120 °C [47]. The membrane even maintained a high selectivity of 90 under a high feed gas pressure of 9.5 bar ($\Delta P = 8.5$ bar). The separation factor dropped from 180 to 90 when the feed pressure increased from 1 to 9.5 bar and the permeance of C_3H_6 dropped from 45 to 27.5 GPU with increasing pressure, while the value for C_3H_8 remained very small (about 0.3 GPU). This ZIF-8 membrane also showed excellent stability under longer-term operation at 25 °C and 1 bar of feed pressure with a constant separation factor of 160 and C_3H_6 permeance of 50 GPU over 30 d of continuous operation.

The group of Nair continuously developed MOF membranes using the same fabrication method for ZIF-90 membranes on carbon hollow fibers fabricated via pyrolytic conversion of crosslinked polymer hollow fibers. The gas separation performance of ZIF-90/carbon membranes and ZIF-8/PAI fiber membranes was reported [3,4]. The results show a sharp permeability cut-off between C_3H_6 and C_3H_8 indicating an effective aperture size close to 4.2 Å for ZIF-8. ZIF-90 membranes showed similar molecular separation performance to ZIF-8, However, a significant permeability drop associated with "molecular sieving" is observed at much larger kinetic diameters (around 5.0 Å) for ZIF-90 which would be more suitable for the n-C_4H_{10}/i-C_4H_{10} (4.3 Å/5.0 Å) system [3].

Ultrathin ZIF-8 membranes (200 nm) were prepared by a fast electrochemical process (20 min without using high pressure autoclave) grown on an anodic aluminum oxide (AAO) disc with a Pt coating [49]. The highest propylene/propane selectivity (350) of this type of ZIF-8 membranes was reported. The C_3H_6 permeance decreased with increasing temperature (54 to 28 GPU at 25 to 150 °C), while the C_3H_8 permeance slightly increased, leading to lower separation factors from 350 to 180. Long-term stability of the ZIF-8 membrane (grown for 20 min) for C_3H_6/C_3H_8 separation (~45 GPU and ~300 of selectivity) at room temperature and 1 bar was also described in this paper. This method used a solvent (methanol) and an electrolyte (support) to improve the conductivity of the solution. It also required limited modification of the support, while a conductive layer was still required.

Hou et al. prepared a series of Zn/Co ZIF membranes via a one-step within 20 min using the same method, by introducing Zn^{2+} into the precursor solution of ZIF-67 (100% Co) membranes. The $Zn_{82\%}Co_{18\%}$-ZIF membrane exhibited one of the best C_3H_6/C_3H_8 separation performances with an ideal selectivity of 200 [57]. Zhao et al. reported a PP-supported ZIF-8 membranes synthesized via fast current-driven synthesis within 1 h. The membranes showed excellent C_3H_6/C_3H_8 separation performance with a separation factor above 120. After bending the flat membrane with a curvature of 92 m^{-1}, the C_3H_6/C_3H_8 separation performance was found to be unchanged [58].

Wei et al. further developed an electrochemical deposition technique using water as the solvent without any electrolyte or modulator addition [50]. The membrane exhibited a C_3H_6 permeance of 182 GPU and a separation factor of 142.

Li et al. fabricated ultrathin ZIF-8 membrane (87 nm) through a gel-vapor deposition (GVD) process [51]. The thin selective layer led to a very high propylene permeance (840 GPU), while a

good propylene/propane selectivity (70) was maintained. They also explored the fabrication of ZIF-8 hollow fiber modules applying the GVD technique. The permeation properties of various gases (C_3H_8, C_3H_6, CH_4, N_2, O_2, CO_2 and H_2) were obtained by the constant-pressure, variable volume method (W-K).

Ma et al. reported the fabrication of ZIF nanocomposite membranes by means of an all-vapor-phase method on a porous support [52]. The supports consisted of an α-alumina microporous substrate coated with a 5 μm γ-alumina mesoporous layer with pores in the 2–5 nm range. Firstly, ZnO was deposited on top and inside the γ-alumina layer. This ZnO-alumina composite was rendered essentially impermeable and not selective for propylene/propane, while after ligand-vapor (2-methylimidazole) treatment, it was partially transformed to ZIF and showed stable separation performance. ZIF membranes had the best result of 3×10^{-8} mol·m^{-2}·s^{-1}·Pa^{-1} and 150 of C_3H_6/C_3H_8 separation factor for single gas at 4 atm [52].

Kwon et al. designed a three-component architecture (ZIF-8@ZIF-67@ZIF-8) membranes for C_3H_6/C_3H_8 separation [53]. The authors considered that the tertiary growth of ZIF-8 could heal potential defects occurring in the ZIF-67 surface layer and at the grain boundary allowing a multiple hetero-epitaxial growth enhancing the selectivity up to 200, while the C_3H_6 permeance was of 370×10^{-10} mol·m^{-2}·s^{-1}·Pa^{-1}.

Ramu et al. studied the effect of zinc salts on the microstructure of ZIF-8 seed layers prepared under microwave irradiation, as well as subsequent secondary grown ZIF-8 membranes [54]. Among zinc nitrate hexahydrate ($Zn(NO_3)_2$), anhydrous zinc chloride ($ZnCl_2$) and zinc acetate dihydrate ($Zn(CH_3COO)_2$), zinc nitrate seed layers (densely packed with uniform small crystals around 100–200 nm) produced the best seed layer microstructure leading to subsequent growth. The results showed the best propylene/propane separation performance with an average propylene permeance of 270×10^{-10} mol·Pa^{-1}·m^{-2}·s^{-1} and an average propylene/propane separation factor of 105 for the $Zn(NO_3)_2$–$Zn(NO_3)_2$ membrane.

The group of Koros predicted that neat Zr-fum-fcu-MOF membranes should exhibit a C_3H_6/C_3H_8 selectivity as high as 1130 with a C_3H_6 permeability of 40 Barrer by a back-calculation method [59]. These values are taken as the ideal and theoretical separation performance of membranes reported so far. Unfortunately, these neat Zr-fum-fcu-MOF membranes are still unsuccessful to fabricate.

It is noted that the separation performance of well-intergrown polycrystalline ZIF-8 membranes is determined not only by the selective intracrystalline diffusion (intrinsic material property), but also by nonselective intercrystalline diffusion (grain boundary structure) [53]. The microstructures of polycrystalline membranes however are highly influenced by the processing techniques (preparation method, process control and process conditions). The gas separation performances of ZIF-8 or other MOF membranes are function of the preparation technique (membrane thickness) and the permeation test method. Various methods have been reported, including secondary growth (S-G), counter-diffusion (C-D), interfacial microfluidic membrane processing (IMMP), electrochemical deposition (C-E) and gel vapor deposition (GVD). For secondary growth, nanosized ZIF-8 crystals are typically pre-coated onto the support as a seeding layer acting as a nucleation center. Then, ZIF-8 crystal seeds grow into a dense and continuous membrane by hydro- or solvo-thermal synthesis. Therefore, it is relatively easy to control the membrane structure including composition, thickness, orientation and reproducibility. Both the C-D and IMMP methods can be seen as in situ techniques, but the

electrochemical approach needs a conductive layer to work which is a limitation for commercial application.

Table 6 shows that the thinner the MOF layer, the better the results for the fabrication via electrochemical deposition and GVD. However, ZIF-8 membranes by IMMP on a polymer hollow fiber have high potential for commercial application because they represent an intermediate/combination between the properties of polymers and ZIF membranes. But the gas permeation results depend on the preparation methods, as well as the thickness and number of defects affecting the permeance and selectivity. However, the membrane performance is essentially determined by the MOF structure, such as the pore size with respect to the size of the molecules to be separated.

Most of the permeation tests on MOF membranes were carried out by the Wicke-Kallenbach (W-K) technique (Table 6) which is a constant pressure, variable volume method. Atmospheric pressure was applied to both sides of the permeation cell. The feed side was fed with a propylene/propane gas mixture. On the permeate side, helium or nitrogen were used as sweep gas. The compositions (feed and permeate) were determined on-line via gas chromatography. In general, the feed pressure used for flat MOF membrane is low because of the fragile nature of MOF membranes. On the other hand, the gas transport properties of polymer-based membranes were measured by the time-lag method which is a variable pressure, constant volume method. A single gas or a mixture thereof is fed at a pressure which can be high (for example 40 bar), while the permeate side pressure starts under vacuum an then increases with time. No comparison was done between these two methods.

The data of MOF membranes were summarized in Table 6. Most of the data were obtained at low pressure except for ref. [44,45]. As expected, the separation performances are highly influenced by pressure. For example, the C_3H_6/C_3H_8 selectivity dropped from 180 to 90, while the permeance of C_3H_6 dropped from 45 to 27.5 GPU, when the test pressure increased from 1 to 9.5 bar [44,45]. So these data could not be compared with other polymer-based membrane under higher pressure.

The C_3H_6/C_3H_8 separation performance of membranes produced using different fabrication methods is shown in Figure 6. The best performance is beyond the 2020 experimentally observed C_3H_6/C_3H_8 upper bound of polymer-based membranes [1]. But again, due to the fragile nature of ZIF-8 (MOF) membranes and their difficult preparation, they are far from being used on an industrial scale. Therefore, MOF membranes were developed based on different preparation methods to meet the requirements of industrial applications for many years. The other disadvantages of MOF membranes are (1) the higher costs compared to neat polymer membranes because expensive materials and complex fabrication processes are used, (2) MOF membrane areas (contact area) are relatively small, and (3) MOF membranes need support materials such as polymer hollow fibers or inorganic disks.

3.3. Facilitated transport

Facilitated transport membranes have different structures such as supported liquid membranes, ion exchange membranes and polymer electrolyte membranes. Microporous membranes are chosen as the support, which are immersed into the carrier solution (such as silver nitrate). The main problem is related to the poor stability of the silver nitrate solution in the membrane pores limiting the practical application of supported liquid membranes [60]. Ion exchange membranes are usually

prepared by introducing silver salts into polymer membranes with an acid group (such as sulfonic acid groups), and then the proton is exchanged by the silver ion. To perform the ion exchange, the polymer is immersed in a solution containing silver or other metal salt solution. The silver ions are strongly bound to the anions without water leading to difficult interactions with olefins [61].

A polymer electrolyte membrane (PEM) is composed of a polymer matrix and metal salt distributed in the polymer. Silver ions are fixed by the oxygen atoms in the polymer via coordination. When the olefin permeates through the membrane, the olefin can form coordination complexation with the silver ions and hop to another neighboring silver ion. After several jump along the silver ions, the olefin can be released on the downstream side of the membrane (Figure 1). In contrast, the paraffin cannot complex with silver ions, leading to the preferential permeation of olefins through the membrane. Among these processes, the use of solid polymer electrolytes as facilitated olefin transport membranes is the most promising [9].

Hsiue and Yang prepared three membranes for propylene/propane separation: linear low density polyethylene (LLDPE), LLDPE modified by poly(ethylene-graft-acrylic acid) (PE-g-AA) and PE-g-AA incorporated silver ions (PE-g-AA-Ag^+) [62]. The separation performances were very poor for LLDPE and PE-g-AA membranes as the selectivity was around unity at 40 ℃. The results of complex PE-g-AA-Ag^+ membrane showed a selectivity of 5.5 and a permeability of 1.05 Barrer at 30 ℃ and 1.3 bar under a 45/55 propylene/propane ratio.

Pinnau et al. [63] prepared PEO–AgBF4 (67 wt% $AgBF_4$) composite membrane of 5 μm thickness, where PEO is poly(ethylene oxide) and $AgBF_4$ is silver tetrafluoroborate. Pure gas permeation properties of PEO/$AgBF_4$ composite membranes containing more than 50 wt% $AgBF_4$ in the polymer matrix were excellent as the selectivity was above 1000 for both ethylene/ethane and propene/propane at 23 ℃ and 100 psi, while the values were only 1.2 and 2.5 for a neat PEO membrane. However, the ethylene/ethane selectivity dropped to 240 for the PEO/$AgBF_4$ membrane using a dry feed gas mixture. Unfortunately, no result was reported for the propylene/propane gas mixture.

Kang et al. [64] compared the long-term stability of PEM for propylene/propane mixtures separation. The membranes were based on $AgBF_4$ dissolved in poly(ethylene phthalate) (PEP) and poly(2-ethyl-2-oxazoline) (POZ). The result showed that PEP/$AgBF_4$ membranes performed much better than POZ/$AgBF_4$. The selectivity of propylene/propane and C_3H_6 permeance of PEP/$AgBF_4$ membranes was 55 and 5-6 GPU, while the selectivity drop from 52 to 30 and the permeance from 16 to 5 GPU for POZ/$AgBF_4$ when the test lasted for 150 h at 40 psig and 20 ℃. The authors associated this difference to the very strong coordination interaction between silver ions and the phthalate groups of PEP.

When polymer-silver salt complex membranes are exposed to UV irradiation, the separation performances (permeance and selectivity for propylene/propane) decreased. This behavior is mainly attributed to the reduction of silver ions to silver nanoparticles in the membranes. Kim et al. [65] studied the effect of the polymer matrix on the formation of silver nanoparticles in the polymer-silver salt complex membranes. Three different carbonyl groups were compared: poly(vinyl pyrrolidone) (PVP) with an amide group, poly(vinyl methyl ketone) (PVMK) with a ketone group and poly(methyl methacrylate) (PMMA) with an ester group. The reduction rate of the silver ions had the following order: PVP > PVMK > PMMA, while the size and the distribution of the nanoparticles followed the reverse order.

Pollo et al. [66] prepared PEM membranes (200 μm thick) using polyurethane (PU) and two different silver salts: triflate (CF_3SO_3) and hexafluorantimonate (SbF_6). The results for propylene/propane pure gas are shown in Table 7 for 2 bar and 25 °C (Table 7).

Table 7. Gas permeability and ideal selectivity of propylene and propane through PEM of PU and PIM-1 membranes.

Membrane	P_{C3H6} (Barrer)	P_{C3H8} (Barrer)	$\alpha_{C3H6/C3H8}$	Test conditions (°C/bar)	Ref.
PU	191.5	91.6	2.1	25/2	[66]
PU/$AgCF_3SO_3$ (20% w/w)	188.1	18.0	10.4	25/2	[66]
PU/$AgSbF_6$ (20% w/w)	50.1	7.7	6.5	25/2	[66]
PIM-1	2534	851	3.0	35/3.5	[67]
cPIM	421	44.7	9.4	35/3.5	[67]
ZncPIM	837	80.9	10.4	35/3.5	[67]
AgcPIM	759	64.9	11.7	35/3.5	[67]
MgcPIM	568	37.3	15.2	35/3.5	[67]

Wang et al. reported a novel method to make polymer electrolyte PEI/Pebax2533/$AgBF_4$ composite membranes: PEI as the supporting substrate, a thin layer of Pebax2533 (polyether block amide) on the microporous PEI by dip-coating and finally the external surface of PEI/Pebax2533 composite membrane by immersion into an $AgBF_4$ aqueous solution (concentration from 1 to 8 mol/L) for 2 h, while the other side of the composite membrane should not be in contact with the $AgBF_4$ aqueous solution [61]. The PEI/Pebax2533 composite membrane showed relatively high permeance (above 100 GPU) and low selectivity (~2) for propylene and propane pure gas. But the PEI/Pebax2533/$AgBF_4$ composite membranes had a propylene permeance from 22.6 to 32.4 GPU, while a rapid increase of propylene/propane selectivity was observed reaching more than 1000 (only for pure gas) when the membranes were prepared with 5.0 mol/L and 8.0 mol/L $AgBF_4$ solutions. However, long-term stability and performance of gas mixtures were not reported [68].

Liao et al. [67] compared PEM membranes based on PIM-1 as the polymer matrix (with intrinsic microporosity) incorporated with various metal ions such as Zn^{2+}, Mg^{2+} and Ag^{+}. The pure gas transport properties of C_3H_6 and C_3H_8 were tested at 3.5 atm and 35 °C by a variable-pressure constant-volume gas permeation cell (Table 7). The PIM-1 membrane was dried in a vacuum oven at 120 °C for 24 h, while the hydrolyzed PIM-1 membrane was denoted as cPIM. The metal ion treated membranes had higher C_3H_6/C_3H_8 selectivity than cPIM because the metal-carboxyl complex may enhance the C_3H_6 sorption and facilitate C_3H_6 transport. Unfortunately, no results on gas mixture and long-term stability were reported.

Silver polymer electrolyte membranes were shown to have good selectivity and separation performance for propylene/propane mixture. However, their industrial application is significantly hampered because of the poor stability of the silver ions carrier. Silver ions are known to react with other substances or be deactivated by light exposure (silver nanoparticle or elemental) resulting in a sharp decrease in membrane performances. Kang et al. suggested that the addition of nanoparticles into a polymeric matrix is a good way to delay the reduction of silver ions to improve mass transport [67].

Kang et al. [69] added nanoparticles (TiO_2 and Al_2O_3) into a polymeric matrix (poly(2-ethyl-2-oxazoline) (POZ) and $AgNO_3$) to improve mass transport. The best result was a C_3H_6 permeance of 0.5 GPU and a selectivity of 7 for 0.15 mol ratio TiO_2 in POZ/$AgNO_3$ PEM. Kang et al. [70] then

introduced $Al(NO_3)_3$ into a POZ/$AgBF_4$ membrane. Comparing the performance of the POZ/$AgBF_4$, both the selectivity of propylene over propane and the mixed gas permeance decreased over time due to the reduction of silver ions to silver metal nanoparticles. Stable silver ions, maintained for more than 14 d, were confirmed by the separation performance of propylene/propane mixtures (selectivity = 21 and permeance = 4.8 GPU) over time and by the color change of the POZ/$AgBF_4$/$Al(NO_3)_3$ complex. The reason is that $Al(NO_3)_3$ weakened the interaction between Ag^+ and the functional groups of polymers to reduce the oxidation ability of Ag^+.

Sun et al. [71] introduced titanium dioxide (TiO_2) nanoparticles into PEO/silver tetrafluoroborate polymer electrolyte membranes for propylene/propane separation. The results showed that the propylene/propane selectivity of PEM increased with increasing concentration of silver salt and TiO_2. However, the propylene/propane selectivity decreased from 19.0 to 5.4 as the silver carrier ions became deactivated over the course of 196 h of experiment.

Poly(vinyl alcohol) (PVA)/$AgBF_4$/$Al(NO_3)_3$ complex membrane for propylene/propane separation was developed by Park et al. [72]. The selectivity and permeance of the membranes were determined to be 17 and 11 GPU at 3 bar and room temperature. Interestingly, the propylene/propane separation performance was maintained for more than 145 h at room temperature even though the Ag ions, which functioned as olefin carriers, were observed to be unstable during this period. For PVA/$AgBF_4$ membrane without $Al(NO_3)_3$, the selectivity dropped from 8 to 1.2 in only 25 h due to the conversion of Ag ions into inactive nanoparticles. Further permeance increases after this decrease around 25 h was attributed to interfacial defects between the PVA chains and the Ag nanoparticles generated.

Zarca et al. described a versatile approach to improve the complex mobile/fixed hybrid mechanism inside composite membranes [73]. The authors deduced a mathematical expression for the "effective permeability" of propylene by the fixed carrier mechanism. The model was checked by comparing simulated and experimental permeation data for propylene/propane gas mixtures in PVDF-HFP/Ag^+ (PVDF-HFP, poly(vinylidene fluoride-co-hexafluoropropylene)). These membranes had interesting performance giving propylene permeability as high as 1800 Barrer with propylene/propane selectivity up to 300. The authors considered that this model will be a valuable tool for future design and optimization of more complex propylene/propane separation systems for more efficient process configurations.

Pebax-1657/$AgBF_4$/$Al(NO_3)_3$ electrolyte membranes were prepared for C_3H_6/C_3H_8 separation by Jeong et al. [74]. Pebax-1657, having 40% amide groups and 60% ether linkages, was selected as the polymer matrix. The selectivity and mixed-gas permeance of the membrane were 8.8 and 22.5 GPU. The selectivity of PVP/$AgBF_4$/$Al(NO_3)_3$ membranes was reported to be 15.0 with a permeability of 1.3 GPU [75].

Jung et al. [76] reported Pebax-5513/$AgBF_4$/$Al(NO_3)_3$ membranes to compare with Pebax-1657 as Pebax-5513 has an amide groups content to 60% in the copolymer. The selectivity and permeance of the membranes were 7.7 and 11.1 GPU. Unexpectedly, the membrane selectivity was not improved, while the permeance was decreased.

Pebax-2533, with 80% ether group and 20% amide group, was used by Kim et al. to prepare polyether-block-amide (Pebax)-2533/metal salt/Al salt membranes for mixed olefin/paraffin separation [77]. In this case, the Al salts were also used to stabilize the metal ions. High permeance was expected due to the high proportion of ether groups since these functional groups provide relatively permeable regions. The results showed that the Pebax-2533 composite membrane had a

propylene/propane selectivity of 5 with 10 GPU for propane. The permeance was not unexpectedly improved and the selectivity was reduced compared to Pebax-1657/$AgBF_4$/$Al(NO_3)_3$ electrolyte membranes [74].

Table 8. Performance of PEM membranes for C_3H_6/C_3H_8 gas mixture separation.

Membrane	C_3H_6/C_3H_8 mixture	Permeance C_3H_6 (GPU)	C_3H_6/C_3H_8 selectivity	Test condition (bar/°C)	Thickness (μm)	Ref.
PEP/$AgBF_4$	50/50	5-6	55	2.7/20	10	[64]
POZ/$AgBF_4$	50/50	16	52	2.7/20	10	[64]
PVP/$AgBF_4$/Al $(NO_3)_3$	-	1.3	15	-	-	[75]
(PVA)/$AgBF_4$/$Al(NO_3)_3$	50/50	11	17	3/RT	23	[72]
PVDF-HFP/$AgBF_4$	50/50	25	300	2/30	71	[73]
Pebax-1657/$AgBF_4$/$Al(NO_3)_3$	50/50	8.8	22.5	-	1.4	[74]
PEBAX-5513/$AgBF_4$/$Al(NO_3)_3$	50/50	7.7	11.1	1/RT	3.2	[76]
PEBAX-2533/$AgBF_4$/$Al(NO_3)_3$	50/50	5	10	1/RT	3.3	[77]
PVP/$AgCF_3SO_3$/$Al(NO_3)_3$	50/50	0.5	5	1/RT	2.7	[78]
PEOx/$AgBF_4$	50/50	36	65	2.8/23	1	[79]
PEOx/$AgCF_3SO_3$	50/50	32	19	2.8/23	1	[79]
PVP/$AgBF_4$	50/50	36	65	2.8/23	1	[79]
PVP/$AgCF_3SO_3$	50/50	28	18	2.8/23	1	[79]
PDMS/57wt.$AgBF_4$	50/50	13	150	-	2	[80]

Park et al. studied the long-term stability of PVP/$AgCF_3SO_3$/$Al(NO_3)_3$ complex membranes [78]. The results showed that the best separation performance was a selectivity of 5 and a permeance of 0.5 GPU for mixed gas for the 1/1/0.004 PVP/$AgCF_3SO_3$/$Al(NO_3)_3$ membrane, while the selectivity and permeance remained constant for up to 100 h. This work showed that the color of the PVP/$AgCF_3SO_3$/$Al(NO_3)_3$ membrane remained white even after being kept at room temperature for over five days, but then changed from white to light brown after 11 days. For the PVP/$AgCF_3SO_3$ complex without $Al(NO_3)_3$, the membrane became dark-brown after only 5 d indicating that the Ag^+ ions were partially converted into silver nanoparticles [76]. The results were similar to previous works on PEM [79,80].

Table 8 compares the properties of facilitated membranes. It can be seen that using PEP, POZ, PVDH, PEO and PVP with $AgBF_4$, the PEM have better separation performance for C_3H_6/C_3H_8 mix gases. Thinner membranes also show better separation performances.

Silver polymer electrolyte membranes were shown to have good selectivity and separation performance for propylene/propane mixture and Figure 6 presents a comparison of the data available for facilitated transport membranes with respect to the 2020 experimentally observed C_3H_6/C_3H_8 upper bound of polymer-based membranes. However, all the facilitated transport membranes have an important disadvantage due to their long-term instability. For the moment, the most stable membranes were only for two weeks due to silver ions carrier reduction, even when some additives were used to stabilize the metal ions. Therefore, facilitated transport membranes, including PEM, still need some improvement to meet some basic requirements for industrial applications, compared to neat polymer separation modules working continuously for several years.

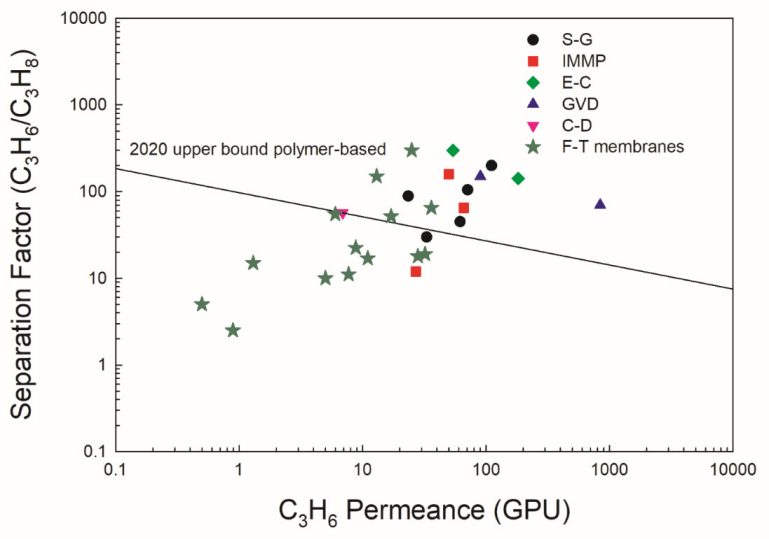

Figure 6. Mix gas C_3H_6/C_3H_8 separation performance of MOF membranes (using different fabrication methods) and facilitated transport (polymer electrolyte) membranes.

4. Conclusion

Generally, polymer-based membranes follow the solution-diffusion mechanism and are not suitable for C_3H_6/C_3H_8 separation because the physico-chemical properties of both gases are too close. In addition, the difference between their molecular dynamic diameters is very small (less than 0.3 Å). In this case, even carbon molecular sieve (CMS) membranes do not lead to selectivities over 100.

For propylene/propane membrane separation, as for any gas separation, stability is very important for industrial applications. So specific problems like carrier stability, plasticization effect and aging effect must be accounted for. Physical aging is a disadvantage of CMS membranes since the micro-pores shrink over time leading to a reduction in permeability. But a regeneration approach for CMS fibers is possible to overcome this problem. The porous structure collapse is another problem for CMS, This is why high glass transition temperature (Tg) materials must be selected for future development, as well as the pyrolysis protocol and hollow fiber formation by using additives. Facilitated transport membranes show excellent propylene/propane mixture separation performances. However, compared with commercial polymeric membranes (2–7 years), the instability of the carriers, including the reduction of Ag^+, are the main challenges limiting their long-term operation and practical applications (1–2 weeks). Although some nanoparticles were used to help stabilize the metal ions, the membrane stability is still not high enough. Finally, plasticization is a concern for polymer-based membranes.

Metal-organic frameworks (MOF) membranes were developed for the separation of olefins and paraffins, some of which (ZIF-8) have achieved quite high separation selectivity reaching 300 for gas mixture. However, such membranes are faced with challenges in terms of low mechanical strength and difficult scale-up fabrication.

Covalent organic frameworks (COF) are a class of porous materials containing light elements (hydrogen, boron, carbon, nitrogen, oxygen and silicon) linked by strong covalent bond. Since COF are light materials having strong covalent bonds, they show low density, good thermal and chemical

stability, and inherent porosity with a well-defined pore aperture, ordered channel structure, large surface area and multi-dimensions. Compared to MOF, 3-D COF can provide a higher fraction of accessible surface area for gas separation [81]. The large-scale production of COF may be developed to advance the design and application of new COF adsorbents to included into membranes with specific structural properties for propylene/propane separation.

The ideal membranes for propylene/propane separation should have easy fabrication, low cost and high efficiency with an appropriate pore size between 4.0–4.3 Å which can be tailored via careful synthesis. Several polystyrene-block-poly(4-vinylpyridine) (PS-b-P4VP) di-block copolymers with different molecular weights were synthesized by Rangou et al. [82]. The pore sizes are between 22–48 nm. So self-organized isoporous membranes could be optimized by the reaction conditions to highly reduce the pore size for gas separation. This is the main challenge for the future, not only for propylene/propane separation.

Although membrane-based technology for propylene and propane was developed, more work is still needed to improve on the results obtained. Future works should include:

(1) Selection of more rigid molecular sieve having suitable pore size, especially covalent organic frameworks (COF) controllable assembly for olefin/paraffin separations at the lab-scale.
(2) Combination of two or more methods (hybrid processes) to fabricate thinner flat membranes or hollow fiber modules, such as IMMP, to put MOF layers on the inside or outside of polymer hollow fibers as the flexible polymer support could improve the membranes stability. Then, prepare spiral wound modules and hollow fiber modules to determine their suitability and overall properties under commercial application conditions; i.e. over a wide range of temperature, pressure and gas concentration.
(3) Study the gas permeation under more realistic feed conditions; i.e. similar to industrial conditions composition.
(4) Improve the long-term stability of facilitated transport membranes and anti-aging CMS membranes.
(5) Modeling of the membrane permeability, selectivity and stability would be helpful to better optimize the properties and reduce the costs of not only olefin/paraffin separations, but any gas separation in general.

Conflict of interest

The authors have no conflict of interest with the publication of this article.

Reference

1. Chen XY, A Xiao A, Rodrigue D (2021) Polymer-based membranes for propylene/propane separation. *Sep Purif Rev* (in press). https://doi.org/10.1080/15422119.2021.1874415
2. Ren YX, Liang X, Dou HZ, et al. (2020) Membrane-based olefin/paraffin separations. *Adv Sci* 7: 2001398. https://doi.org/10.1002/advs.202001398
3. Eum K, Ma C, Rownaghi A, et al. (2016) ZIF-8 Membranes via interfacial microfluidic processing in polymeric hollow fibers: Efficient propylene separation at elevated pressures. *ACS Appl Mater Inter* 8: 25337–25342. https://doi.org/10.1021/acsami.6b08801

4. Eum K, Ma C, Koh DY, et al. (2017) Zeolitic imidazolate framework membranes supported on macroporous carbon hollow fibers by fluidic processing techniques. *Adv Mater Interfaces* 4: 1700080. https://doi.org/10.1002/admi.201700080
5. Koros WJ, Zhang C (2017) Materials for next-generation molecularly selective synthetic membranes. *Nat Mater* 16: 289–297. https://doi.org/10.1038/nmat4805
6. Zhou HC, Long JR, Yaghi OM (2012) Introduction to metal-organic frameworks. *Chem Rev* 112: 673-674. https://doi.org/10.1021/cr300014x
7. Hara N, Yoshimunea M, Negishi H, et al. (2014) Diffusive separation of propylene/propane with ZIF-8 membranes. *J Membrane Sci* 450: 215–223. https://doi.org/10.1016/j.memsci.2013.09.012
8. Zhou HX, Zwanzig R (1991) A rate process with an entropy barrier. *J Chem Phys* 94: 6147–6152. https://doi.org/10.1063/1.460427
9. Kim JH, Won J, Kang YS (2004) Olefin-induced dissolution of silver salts physically dispersed in inert polymers and their applications to olefin/paraffin separation. *J Membrane Sci* 241: 403–407. https://doi.org/10.1016/j.memsci.2004.05.027
10. Zarca R, Ortiz A, Gorri D, et al. (2017) A practical approach to fixed-site-carrier transport modeling for the separation of propylene/propane mixtures through silver containing polymeric membranes. *Sep Purif Technol* 180: 82–89. https://doi.org/10.1016/j.seppur.2017.02.050
11. Hou J, Liu P, Jiang M, et al. (2019) Olefin/paraffin separation through membranes: from mechanisms to critical materials. *J Mater Chem A* 7: 23489–23511. https://doi.org/10.1039/C9TA06329C
12. Kim JH, Kang YS, Won J (2004) Silver polymer electrolyte membranes for facilitated olefin transport: carrier properties, transport mechanism and separation performance. *Macromol Res* 12: 145–55. https://doi.org/10.1007/BF03218383
13. Xu L, Rungta M, Brayden MK, et al. (2012) Olefins-selective asymmetric carbon molecular sieve hollow fiber membranes for hybrid membrane-distillation processes for olefin/paraffin separations. *J Membrane Sci* 423: 314–323. https://doi.org/10.1016/j.memsci.2012.08.028
14. Swaidan RJ, Ma XH, Pinnau I (2016) Spirobisindane-based polyimide as efficient precursor of thermally rearranged and carbon molecular sieve membranes for enhanced propylene/propane separation. *J Membrane Sci* 520: 983–989. https://doi.org/10.1016/j.memsci.2016.08.057
15. Fuertes AB, Menendez I (2002) Separation of hydrocarbon gas mixtures using phenolic resin-based carbon membranes. *Sep Purif Technol* 28: 29–41. https://doi.org/10.1016/S1383-5866(02)00006-0
16. Kiyono M, Williams PJ, Koros WJ (2010) Effect of pyrolysis atmosphere on separation performance of carbon molecular sieve membranes. *J Membrane Sci* 359: 2–10. https://doi.org/10.1016/j.memsci.2009.10.019
17. Suda H, Haraya K (1997) Alkene/alkane permselectivities of a carbon molecular sieve membrane. *Chem Commun* 1: 93–94. https://doi.org/10.1039/a606385c
18. Steel KM, Koros WJ (2003) Investigation of porosity of carbon materials and related effects on gas separation properties. *Carbon* 41: 253–266. https://doi.org/10.1016/S0008-6223(02)00309-3
19. Steel KM, Koros WJ (2005) An investigation of the effects of pyrolysis parameters on gas separation properties of carbon materials. *Carbon* 43: 1843–1856. https://doi.org/10.1016/j.carbon.2005.02.028

20. Xu L, Rungta M, Koros WJ (2011) Matrimid® derived carbon molecular sieve hollow fiber membranes for ethylene/ethane separation. *J Membrane Sci* 380: 138–147. https://doi.org/10.1016/j.memsci.2011.06.037
21. Bhuwania N, Labreche Y, Achoundong CSK, et al. (2014) Engineering substructure morphology of asymmetric carbon molecular sieve hollow fiber membranes. *Carbon* 76: 417–434. https://doi.org/10.1016/j.carbon.2014.05.008
22. Yerzhankyzy A, Ghanem BS, Wang Y, et al. (2020) Gas separation performance and mechanical properties of thermally-rearranged polybenzoxazoles derived from an intrinsically microporous dihydroxyl-functionalized triptycene diamine-based polyimide. *J Membrane Sci* 595: 117512. https://doi.org/10.1016/j.memsci.2019.117512
23. Smith ZP, Hernandez G, Gleason KL (2015) Effect of polymer structure on gas transport properties of selected aromatic polyimides, polyamides and TR polymers. *J Membrane Sci* 493: 766–781. https://doi.org/10.1016/j.memsci.2015.06.032
24. Karunaweera C, Musselman Jr IH, Balkus KJ (2019) Fabrication and characterization of aging resistant carbon molecular sieve membranes for C3 separation using high molecular weight crosslinkable polyimide, 6FDA-DABA. *J Membrane Sci* 581: 430–438. https://doi.org/10.1016/j.memsci.2019.03.065
25. 25. Okamoto K, Kawamura S, Yoshino M, et al. (1999) Olefin/paraffin separation through carbonized membranes derived from an asymmetric polyimide hollow fiber membrane. *Ind Eng Chem Res* 38: 4424–4432. https://doi.org/10.1021/ie990209p
26. Askari M, Yang T, Chung TS (2012) Natural gas purification and olefin/paraffin separation using cross-linkable dual-layer hollow fiber membranes comprising β-Cyclodextrin. *J Membrane Sci* 423–424: 392–403. https://doi.org/10.1016/j.memsci.2012.08.036
27. Hayashi J, Mizuta H, Yamamoto M, et al. (1996) Separation of ethane/ethylene and propane/propylene systems with a carbonized BPDA-p,p'-ODA polyimide membrane. *Ind Eng Chem Res* 35: 4176–4181. https://doi.org/10.1021/ie960264n
28. Ma XL, Lin BK, Wei XT (2013) Gamma-alumina supported carbon molecular sieve membrane for propylene/propane separation. *Ind Eng Chem Res* 52: 4297–4305. https://doi.org/10.1021/ie303188c
29. Ma XL, Williams S, Wei XT, et al. (2015) Propylene/propane mixture separation characteristics and stability of carbon molecular sieve membranes. *Ind Eng Chem Res* 54: 9824–9831. https://doi.org/10.1021/acs.iecr.5b02721
30. Xu LR, Rungta M, Hessleret J, al. (2014) Physical aging in carbon molecular sieve membranes. *Carbon* 80: 155–166. https://doi.org/10.1016/j.carbon.2014.08.051
31. Kim SJ, Lee PS, Chang JS, et al. (2018) Preparation of carbon molecular sieve membranes on low-cost alumina hollow fibers for use in C_3H_6/C_3H_8 separation. *Sep Purif Technol* 194: 443–450. https://doi.org/10.1016/j.seppur.2017.11.069
32. Ma X, Lin YS, Wei X, et al. (2016) Ultrathin carbon molecular sieve membrane for propylene/propane separation. *AIChE J* 62: 491–499. https://doi.org/10.1002/aic.15005
33. Teixeira M, Campo MC, Tanaka DAP, et al. (2011) Composite phenolic resin-based carbon molecular sieve membranes for gas separation. *Carbon* 49: 4348–4358. https://doi.org/10.1016/j.carbon.2011.06.012

34. Qiu WL, Vaughn J, Liu GP, et al. (2019) Hyperaging tuning of a carbon molecular-sieve hollow fiber membrane with extraordinary gas-separation performance and stability. *Angew Chem Int Ed* 58: 11700–11703. https://doi.org/10.1002/anie.201904913
35. Qiu WL, Xu L, Liu Z, et al. (2021) Surprising olefin/paraffin separation performance recovery of highly aged carbon molecular sieve hollow fiber membranes by a super-hyperaging treatment. *J Membrane Sci* 620: 118701. https://doi.org/10.1016/j.memsci.2020.118701
36. Guo M, Kanezashi M, Nagasawa H, et al. (2020) Pore subnano-environment engineering of organosilica membranes for highly selective propylene/propane separation. *J Membrane Sci* 60: 117999. https://doi.org/10.1016/j.memsci.2020.117999
37. Guo M, Kanezashi M, Nagasawa H, et al. (2020) Fine-tuned, molecular-composite, organosilica membranes for highly efficient propylene/propane separation via suitable pore size. *AIChE J* 66: e16850. https://doi.org/10.1002/aic.16850
38. Chu YH, Yancey D, Xu L, et al. (2018) Iron-containing carbon molecular sieve membranes for advanced olefin/paraffin separations. *J Membrane Sci* 548: 609–620. https://doi.org/10.1016/j.memsci.2017.11.052
39. Shin JH, Yu HJ, Park J, et al. (2020) Fluorine-containing polyimide/polysilsesquioxane carbon molecular sieve membranes and techno-economic evaluation thereof for C_3H_6/C_3H_8 separation. *J Membrane Sci* 598: 117660. https://doi.org/10.1016/j.memsci.2019.117660
40. Mundstock A, Wang N, Friebe S (2015) Propane/propene permeation through Na-X membranes: The interplay of separation performance and pre-synthetic support functionalization. *Micropor Mesopor Mat* 215: 20–28. https://doi.org/10.1016/j.micromeso.2015.05.019
41. André V, Quaresma S, Ferreira da Silva JL, et al. (2017) Exploring mechanochemistry to turn organic bio-relevant molecules into metal-organic frameworks: a short review. *Beilstein J Org Chem* 13: 2416–2427. https://doi.org/10.3762/bjoc.13.239
42. Katsenis AD, Puškarić, A, Štrukil V, et al. (2015) In situ X-ray diffraction monitoring of a mechanochemical reaction reveals a unique topology metal-organic framework. *Nat Commun* 6: 1–8. http://doi.org/:10.1038/ncomms7662
43. Available from: http://www.chemtube3d.com. 2022.
44. Pan Y, Li T, Lestari G, et al. (2012) Effective separation of propylene/propane binary mixtures by ZIF-8 membranes. *J Membrane Sci* 390–391: 93–98. https://doi.org/10.1016/j.memsci.2011.11.024
45. Pan Y, Liu W, Zhao Y, et al. (2015) Improved ZIF-8 membrane: Effect of activation procedure and determination of diffusivities of light hydrocarbons. *J Membrane Sci* 493: 88–96. https://doi.org/10.1016/j.memsci.2015.06.019
46. Liu C, Ma D, Xi X, et al. (2014) Gas transport properties and propylene/propane separation characteristics of ZIF-8 membranes. *J Membrane Sci* 451: 85–93. https://doi.org/10.1016/j.memsci.2013.09.029
47. Eum K, Ma C, Rownaghi A, et al. (2016) ZIF-8 membranes via interfacial microfluidic processing in polymeric hollow fibers: Efficient propylene separation at elevated pressures. *ACS Appl Mater Interf* 8: 25337–25342. https://doi.org/10.1021/acsami.6b08801
48. Eum K, Rownaghi A, Choi D, et al. (2016) Fluidic processing of high-performance ZIF-8 membranes on polymeric hollow fibers: Mechanistic insights and microstructure control. *Adv Funct Mater* 26: 5001–5018. https://doi.org/10.1002/adfm.201601550

49. Zhou S, Wei Y, Li L, et al. (2018) Paralyzed membrane: Current-driven synthesis of a metal-organic framework with sharpened propene/propane separation. *Sci Adv* 4: 1393. https://doi.org/10.1126/sciadv.aau1393
50. Wei R, Chi HY, Li X, et al. (2020) Aqueously cathodic deposition of ZIF-8 membranes for superior propylene/propane separation. *Adv Funct Mater* 30: 1907089. https://doi.org/10.1002/adfm.201907089
51. Li W, Su P, Li Z, et al. (2017) Ultrathin metal-organic framework membrane production by gel-vapour deposition. Nat Commun 8: 406. https://doi.org/10.1038/s41467-017-00544-1
52. Ma X, Kumar P, Mittal N, et al. (2018) Zeolitic imidazolate framework membranes made by ligand-induced permselectivation. *Science* 361: 1008–1011. https://doi.org/10.1126/science.aat4123
53. Kwon HT, Jeong HK, Lee AS, et al. (2015) Heteroepitaxially grown zeolitic imidazolate framework membranes with unprecedented propylene/propane separation performances. *J Am Chem Soc* 137: 12304–12311. https://doi.org/10.1021/jacs.5b06730
54. Ramua G, Leea MJ, Jeong HK (2018) Effects of zinc salts on the microstructure and performance of zeoliticimidazolate framework ZIF-8 membranes for propylene/propane separation. *Micropor Mesopor Mat* 259: 155–162. https://doi.org/10.1016/j.micromeso.2017.10.010
55. Kwon HY, Jeong HK (2013) In situ synthesis of thin zeolitic-imidazolate framework ZIF-8 membranes exhibiting exceptionally high propylene/propane separation. *J Am Chem Soc* 135: 10763–10768. https://doi.org/10.1021/ja403849c
56. Brown AJ, Brunelli NA, Eum K, et al. (2014) Interfacial microfluidic processing of metal-organic framework hollow fiber membranes. *Science* 345: 72–75. https://doi.org/10.1126/science.1251181
57. Hou Q, Zhou S, Wei Y, et al. (2020) Balancing the grain boundary structure and the framework flexibility through bimetallic metal-organic framework (MOF) membranes for gas separation. *JACS* 142: 9582–9586. https://doi.org/10.1021/jacs.0c02181
58. Zhao Y, Wei Y, Lyu L, et al. (2020) Flexible polypropylene-supported ZIF-8 membranes for highly efficient propene/propane separation. *JACS* 142: 20915–20919. https://doi.org/10.1021/jacs.0c07481
59. Liu Y, Chen ZJ, Liu GP (2019) Conformation-controlled molecular sieving effects for membrane-based propylene/propane separation. *Adv Mater* 31: 1807513. https://doi.org/10.1002/adma.201807513
60. Fallanza M, Ortiz A, Gorri D, et al. (2012) Experimental study of the separation of propane/propylene mixtures by supported ionic liquid membranes containing Ag^{+}-RTILs as carrier. *Sep Purif Technol* 97: 83–89. https://doi.org/10.1016/j.seppur.2012.01.044
61. Kang SW, Char K, Kang YS (2008) Novel application of partially charged silver nanoparticles for transport in olefin/paraffin separation membranes. *Chem Mater* 20: 1308–1311. https://doi.org/10.1021/cm071516l
62. Hsiue GH, Yang JS (1993) Novel methods in separation of olefin/paraffin mixtures by functional polymeric membranes. *J Membrane Sci* 82: 117–128. https://doi.org/10.1016/0376-7388(93)85097-G

63. Pinnau I, Toy LG (2001) Solid polymer electrolyte composite membranes for olefin/paraffin separation. *J Membrane Sci* 184: 39–48. https://doi.org/10.1016/S0376-7388(00)00603-7
64. Kang SW, Kim JH, Oh KS, et al. (2004) Highly stabilized silver polymer electrolytes and their application to olefin transport membranes. *J Membrane Sci* 236: 163–169. https://doi.org/10.1016/j.memsci.2004.02.020
65. Kim JH, Min B, Won J, et al. (2006) Effect of the polymer matrix on the formation of silver nanoparticles in polymer-silver salt complex membranes. *J Polym Sci Pol Phys* 44: 1168–1178. https://doi.org/10.1002/polb.20777
66. Pollo LD, Durate LT, Anacleo M, et al. (2012) Polymeric membranes containing silver salts for propylene/propane separation. *Brazil J Chem Eng* 29: 307–314. https://doi.org/10.1590/S0104-66322012000200011
67. Liao KS, Lai JY, Chung TS (2016) Metal ion-modified PIM-1 and its application for propylene/propane separation. *J Membrane Sci* 515: 36–44. https://doi.org/10.1016/j.memsci.2016.05.032
68. Wang Y, Ren J, Deng M (2011) Ultrathin solid polymer electrolyte PEI/Pebax2533/$AgBF_4$ composite membrane for propylene/propane separation. *Sep Purif Technol* 77: 46–52. https://doi.org/10.1016/j.seppur.2010.11.018
69. Kang SW, Bae W, Kim JH, et al. (2009) Behavior of inorganic nanoparticles in silver polymer electrolytes and their effects on silver ion activity for olefin transport. *Ind Eng Chem Res* 48: 8650–8654. https://doi.org/10.1021/ie9000103
70. Kang SW, Kim JH, Won J, et al. (2013) Suppression of silver ion reduction by $Al(NO_3)_3$ complex and its application to highly stabilized olefin transport membranes. *J Membrane Sci* 445: 156. https://doi.org/10.1016/j.memsci.2013.06.010
71. Sun HX, Ma C, Wang T, et al. (2014) Satellite TiO_2 nanoparticles induced by silver ion in polymer electrolytes membrane for propylene/propane separation. *Mater Chem Phys* 148: 790–797. https://doi.org/10.1016/j.matchemphys.2014.08.050
72. Park YS, Chun S, Kang YS, et al. (2017) Durable poly(vinyl alcohol)/$AgBF_4$/$Al(NO_3)_3$ complex membrane with high permeance for propylene/propane separation. *Sep Purif Technol* 174: 39–43. https://doi.org/10.1016/j.seppur.2016.09.050
73. Zarca R, Ortiz A, Gorri D, et al. (2017) A practical approach to fixed-site-carrier transport modeling for the separation of propylene/propane mixtures through silver containing polymeric membranes. *Sep Purif Technol* 180: 82–89. https://doi.org/10.1016/j.seppur.2017.02.050
74. Jeong S, Sohn H, Kang SW (2018) Highly permeable PEBAX-1657 membranes to have long-term stability for olefin transport. *Chem Eng J* 333: 276–279. https://doi.org/10.1016/j.cej.2017.09.125
75. Yoon KW, Kang SW (2016) Preparation of polyvinyl pyrrolidone/AgBF4/$Al(NO_3)_3$ electrolyte membranes for gas transport. *Membrane J* 26: 38–42. https://doi.org/10.14579/MEMBRANE_JOURNAL.2016.26.1.38
76. Jung KW, Kang SK (2019) Effect of functional group ratio in PEBAX copolymer on propylene/propane separation for olefin transport membranes. *Sci Rep* 9: 11454. https://doi.org/10.1038/s41598-019-47996-7
77. Kim YS, Cho Y, Kang SW (2020) Correlation between functional group and formation of nanoparticles in PEBAX/Ag salt/Al salt complexes for olefin separation. *Polymer* 12: 667. https://doi.org/10.3390/polym12030667

78. Park YS, Kang YS, Kang SW (2015) Cost-effective olefin transport membranes consisting of polymer/AgCF3SO3/Al(NO_3)$_3$ with long-term stability. *J Membrane Sci* 495: 61–64. https://doi.org/10.1016/j.memsci.2015.07.061
79. Yoon Y, Won J, Kang YS (2000) Polymer electrolyte membranes containing silver ion for olefin transport. *Macromolecules* 33: 3185–3186. https://doi.org/10.1021/ma0000226
80. Kim JH, Won J, Kang YS (2004) Olefin-induced dissolution of silver salts physically dispersed in inert polymers and their application to olefin/paraffin separation. *J Membrane Sci* 241: 403–407. https://doi.org/10.1016/j.memsci.2004.05.027
81. Altundal OF, Altintas C, Keskin S (2020) Can COFs replace MOFs in flue gas separation? high-throughput computational screening of COFs for CO_2/N_2 separation. *J Mater Chem A* 8: 14609–14623. https://doi.org/10.1039/D0TA04574H
82. Rangou O, Buhr K, Filiz V (2014) Self-organized isoporous membranes with tailored pore sizes. *J Membrane Sci* 451: 266–275. https://doi.org/10.1016/j.memsci.2013.10.015

AIMS Press